IFGW

UNICAMP

ANO 40

Abstracta

Ano VIII- N. 06

Dez. 06

TRABALHO ACEITO PARA PUBLICAÇÃO

A 009 Experimental realization of suspended atomic chains composed of different atomic species.

TRABALHOS PUBLICADOS

Outubro à Dezembro 2006

P 242 à P 305

TRABALHOS ACEITOS PARA PUBLICAÇÃO

A 009- 06 Experimental realization of suspended atomic chains composed of different atomic species

J. BETTINI, F. SATO, P. Z. COURA, S. O. DANTAS, D. S. GALVAO AND D. UGARTE

Research into nanostructured materials frequently relates to pure substances. This contrasts with industrial applications, where chemical doping or alloying is often used to enhance the electrical or mechanical properties of materials. However, the controlled preparation of doped nanomaterials has been much more difficult than expected because the increased surfacearea- to-volume ratio can, for instance, lead to the expulsion of impurities (self-purification). For nanostructured alloys, the influence of growth methods and the atomic structure on selfpurification is still open to investigation. Here, we explore, experimentally and with molecular dynamics simulations, to what extent alloying persists in the limit that a binary metal is mechanically stretched to a linear chain of atoms. Our results reveal a gradual evolution of the arrangement of the different atomic elements in the narrowest region of the chain, where impurities may be expelled to the surface or enclosed during elongation.

NATURE NANOTECHNOLOGY, accepted on November 2006.

TRABALHO PUBLICADOS

P 242- 06 "A new setup for ground-based measurements of solar activity at 10 mu m"

Melo, A. M., Kaufmann, P., Kudaka, A. S., Raulin, J. P., Marcon, R., Marun, A., Pereyra, P., and Levato, H.

Solar activity measurements in the far- to mid-IR range are receiving renewed interest as part of an effort to complement recent results obtained at submillimeter wavelengths. A new setup has been developed to measure solar activity in the infrared spectral region centered at 10 mu m (30 THz) by means of a camera with focal plane array of uncooled microbolometers. An optical arrangement of concave-convex-concave mirrors magnifies and focuses the full-disk solar image to fit into the field of view of the camera. Techniques were developed to characterize the camera and calibrate the measurements in brightness temperature and flux units. Test observations were made at the Bernard Lyot Solar Observatory, Campinas, Brazil, and were continued at El Leoncito Astronomical Complex, San Juan, Argentina. The sky was found to be almost transparent at 10 mu m at both sites. The first measurements of the solar disk have confirmed the presence of quiescent bright ring, or "plagelike," regions around sunspots, and "disappearances" of sunspots coincident with small soft X-ray bursts. Small mid-IR flares were found, consisting of multiple rapid brightenings (tens of seconds to several minutes) at different locations in the solar active regions, corresponding to soft X-ray bursts reported by GOES satellites. At a wavelength of 10 mu m, the sizes of some flare sources were found to be smaller than the diffraction-limited photometric beam of 25" set by the 10.5 cm diameter objective lens. The intensities of such small mid-IR flares were high, of the order of (8 - 14) x 10(-19) W m(-2) Hz(-1) (or [8 - 14] x 10(4) solar flux units)

***Publications of the Astronomical Society of the Pacific*118[849], 1558-1563. 2006.**

P 243- 06 "Ambient pressure colossal magnetocaloric effect tuned by composition in Mn1-xFexAs"

De Campos, A., Rocco, D. L., Carvalho, A. M. G., Caron, L., Coelho, A. A., Gama, S., Da Silva, L.M., Gandra, F. C. G., dos Santos, A. O., Cardoso, L. P., Von Ranke, P. J., and De Oliveira, N. A

The magnetocaloric effect (MCE) is the basis for magnetic refrigeration, and can replace conventional gas compression technology due to its superior efficiency and environment friendliness(1-3). MCE materials must exhibit a large temperature variation in response to an adiabatic magnetic-field variation and a large isothermal entropic effect is also expected. In this respect, MnAs shows the colossal MCE, but the effect appears under high pressures(4). In this work, we report on the properties of Mn1-xFexAs that exhibit the colossal effect at ambient pressure. The MCE peak varies from 285K to 310K depending on the Fe concentration. Although a large thermal hysteresis is observed, the colossal effect at ambient pressure brings layered magnetic regenerators with huge refrigerating power closer to practical applications around room temperature

***Nature Materials* 5[10], 802-804. 2006.**

P 244- 06 "Antiferromagnetic ordering of divalent Eu in EU3Ir4Sn13 intermetalliccompound"

Ferreira, L. M., Bittar, E. M., Pires, M. A., Urbano, R. R., Aguero, O., Torriani, I., Rettori, C.,Pagliuso, P. G., Malachias, A., Granado, E., Caytuero, A., and Baggio-Saitovich, E.

We report a systematic study of the electronic and magnetic properties of Eu3Ir4Sn13 intermetallic. Single crystals of Eu3Ir4Sn13 were synthesized using a Sn self-flux technique. X-rays powder diffraction shows that this compound crystallizes with the cubic Yb3Rh4Sn13-type structure, space group Pm-3n, which has 40 atoms per unit cell. The Eu ions were found to be divalent and order antiferromagnetically at T-N = 11 K. An additional high-temperature anomaly at T* similar to 50 K is observed in the electrical resistivity and heat capacity data, while it is not obviously present in the magnetic susceptibility. Within the ordered state, a metamagnetic transition is observed at T = 2 K and H-m approximate to 2.7 T when magnetic field is applied along the [100] direction. The evolution of T-N and T* was investigated by electrical resistivity under hydrostatic pressure conditions. We have also carried out electron spin resonance (ESR), and X-ray absorption near edge spectroscopy (XANES) measurements. The role of subtle Eu2+ valence fluctuations and the magnetic correlations in the physical properties of this compound are discussed.

***Physica B-Condensed Matter* 384[1-2], 332-335. 2006.**

P 245- 06 "Band structure and band-gap control in photonic superlattices"

Cavalcanti, S. B., Dios-Leyva, M., Reyes-Gomez, E., and Oliveira, L. E

The photonic band structure as well as the density of photon states of a one-dimensional photonic superlattice comprised of alternate layers of air and GaAs are theoretically investigated within the transfer-matrix formalism. The existence of photonic superlattices of null gap with band-touching phenomena is demonstrated, indicating the importance of one-dimensional photonic superlattices for many important practical applications

***Physical Review B* 74[15]. 2006.**

P 246- 06 "Bosonization approach for bilayer quantum Hall systems at nu(T)=1"

Doretto, R. L., Caldeira, A. O., and Smith, C. M.

We develop a nonperturbative bosonization approach for bilayer quantum Hall systems at nu(T)=1, which allows us to systematically study the existence of an exciton condensate in these systems. An effective boson model is derived and the excitation spectrum is calculated in both the Bogoliubov and the Popov approximations. In the latter case, we show that the ground state of the system is an exciton condensate only when the distance between the layers is very small compared to the magnetic length, indicating that the system possibly undergoes another phase transition before the incompressible-compressible one. The effect of a finite electron interlayer tunneling is included and a quantitative phase diagram is proposed

Physical Review Letters 97[18]. 2006.

P 247- 06 "Bulk photochromism in a tungstate-phosphate glass: A new optical memory material?"

Poirier, G., Nalin, M., Cescato, L., Messaddeq, Y., and Ribeiro, S. J. L.

In this work, we present a new photochromic tungstate based glass which have both absorption coefficient and refractive index modified under laser exposure. The photosensitive effect is superficial under ultraviolet (UV) irradiation but occurs in the entire volume of the glass under visible irradiation. The effect can be obtained in any specific point inside the volume using an infrared femtosecond laser. In addition, the photosensitive phenomenon can be erased by specific heat treatment. This glass can be useful to substitute actual data storage supports and is a promising material for 3-dimensional (3D) and holographic optical storage

Journal of Chemical Physics 125[16]. 2006.

P 248- 06 "Coherent state path integrals in the Weyl representation"

dos Santos, L. C. and de Aguiar, M. A. M.

We construct a representation of the coherent state path integral using the Weyl symbol of the Hamiltonian operator. This representation is very different from the usual path integral forms suggested by Klauder and Skagerstam (1985 Coherent States: Applications in Physics and Mathematical Physics (Singapore: World Scientific)), which involve the normal or the antinormal ordering of the Hamiltonian. These different representations, although equivalent quantum mechanically, lead to different semiclassical limits. We show that the semiclassical limit of the coherent state propagator in the Weyl representation involves classical trajectories that are independent of the width of coherent states. This propagator is also free from the phase corrections found in Baranger et al (2001 J. Phys. A: Math. Gen. 34 7227) for the two Klauder forms and provides an explicit connection between the Wigner and the Husimi representations of the evolution operator

Journal of Physics A-Mathematical and General 39[43], 13465 13482. 2006.

P 249- 06 "Copper-vanadium mixed oxide thin film electrodes"

Souza, E. A., dos Santos, A. O., Cardoso, L. P., Tabacniks, M. H., Landers, R., and Gorenstein,A.

In this work, small amounts of vanadium atoms were incorporated in copper oxide films in order to decrease the charge capacity loss during the electrochemical lithium reaction, mainly in the first cycle. Reactive sputtering was the film deposition technique used to deposit pure copper oxide films, CuO, and copper–vanadium mixed oxides CuO(VOy). The composition, oxidation state and crystallinity of the deposited films were investigated. Electrochemical studies were performed, and the results demonstrated that the mixed oxides have a better electrochemical behavior with a higher capacity and stability in the charge/discharge processes, when compared to the pure CuO films behavior.

Journal of Power Sources 162[1], 679-684. 2006.

P 250- 06 "Correlated electron-hole transitions in bulk GaAs and GaAs-(Ga,Al)As quantum wells: Effects of applied electric and in-plane magnetic fields"

Duque, C. A., Oliveira, L. E., and Dios-Leyva, M.

The effects of crossed electric and magnetic fields on the electronic and exciton properties in semiconductor heterostructures have been investigated within the effective-mass and parabolic band approximations for both bulk GaAs and GaAs-Ga1-xAlxAs quantum wells. The combined effects on the heterostructure properties of the applied crossed electric/magnetic fields together with the direct coupling between the exciton center of mass and internal exciton motions may be dealt with via a simple parameter representing the distance between the electron and hole magnetic parabolas. Calculations lead to the expected behavior for the exciton dispersion in a wide range of the crossed electric/magnetic fields, and present theoretical results are found in good agreement with available experimental measurements

Brazilian Journal of Physics 36[3B], 1038-1041. 2006.

P 251- 06 "Different carbon nanostructured materials obtained in catalytic chemical vapor deposition"

Verissimo, C., Moshkalyov, S. A., Ramos, A. C. S., Goncalves, J. L., Alves, O. L., and Swart, J. W.

Different carbon nanostructured materials, such as nanotubes, nanofibers, nanosprings and nanooctopus, were grown by changing the metal catalyst and experimental parameters of the thermal chemical vapor deposition process. These experiments were performed using a tubular furnace and methane or acetylene as carbon feedstock gases. Thin films of Ni or Cu were deposited onto a SiO2/Si substrate and employed as catalysts. The effect of the growth temperature, metal catalyst and carbon gas precursor (methane or acetylene) on the final carbon nanoestructured material was studied by scanning electron microscopy, Raman spectroscopy and grazing incidence X-ray diffraction. Growth of multiwall carbon nanotubes (MWCNTs) was observed using both metal films and carbon precursor gases, whereas partially oxidized Ni films promoted formation of nanosprings. Experiments with reduced supply of methane resulted in octopus-like carbon nanostructures when a Cu film was used as a catalyst

Journal of the Brazilian Chemical Society 17[6], 1124-1132. 2006.

P 252- 06 "Effects of disorder on the exchange coupling in (Ga,Mn)As diluted magnetic semiconductors"

da Silva, A. J. R., Fazzio, A., dos Santos, R. R., and Oliveira, L. E.

A theoretical study of the effects of disorder on the Mn-Mn exchange interactions for Ga1-xMnxAs diluted magnetic semiconductors is presented. The disorder is intrinsically considered in the calculations, which are performed using an ab initio total energy density-functional approach, for a 128 atoms supercell, and by considering a variety of configurations with 2, 3 and 4 Mn atoms. Results are obtained for the effective J(n)(Mn-Mn), from first (n = 1) all the way up to sixth (n = 6) neighbors via a Heisenberg Hamiltonian used to map the magnetic excitations from ab initio total energy calculations. One then obtains a clear dependence in the magnitudes of n n the J(n)(Mn-Mn) with the Mn concentration x. Moreover, we show that, in the case of fixed Mn concentration, configurational disorder and/or clustering effects lead to large dispersions in the Mn-Mn exchange interactions. Also, calculations for the ground-state total energies for several configurations suggest that a proper consideration of disorder is needed when one is interested in treating temperature and annealing effects

Brazilian Journal of Physics 36[3B], 813-816. 2006.

P 253- 06 "Effects of in-plane magnetic fields on the electronic cyclotron effective mass and Lande factor in GaAs-(Ga,Al)As quantum wells"

Reyes-Gomez, E., Leiva, C. A. P., Oliveira, L. E., and Dios-Leyva, M.

The dependence of the electron Lande g-factor on carrier confinement in quantum wells recently gained both experimental and theoretical interest. The g factor of electrons in GaAs-(Ga,Al)As quantum wells is of special interest, as it changes its sign at a certain value of the well width. In the present work, the effects of an in-plane magnetic field on the cyclotron effective mass and on the Lande g(perpendicular to)-factor in single GaAs-(Ga,Al)As quantum wells are studied. Theoretical calculations are performed in the framework of the effective-mass and non-parabolic-band approximations. The Ogg-McCombe Hamiltonian is used for the conduction-band electrons in the semiconductor heterostructure, and the Lande g(perpendicular to)-factor theoretically evaluated is found in good agrement with available experimental measurements

Brazilian Journal of Physics 36[3B], 858-861. 2006.

P 254- 06 "Effects of magnetic interparticle coupling in the blocking temperature of granular Co multilayers"

Denardin, J. C., Nunes, W. C., and Knobel, M.

In order to study the influence of magnetic interactions on the blocking temperature of magnetic nanoparticles, magnetization measurements were carried out on a discontinuous CO/SiO2 multilayer. The observed field dependence of the blocking temperature does not fit any of the non-interacting laws commonly used to describe this behavior. We applied a generalized model which considers a field-dependent magnetic correlation length. This model explains well the experimental results and can be used in other nanoparticulate systems. (c) 2006 Elsevier B.V. All rights reserved

Physica B-Condensed Matter 384[1-2], 290-293. 2006.

P 255- 06 "Electron g-factor and cyclotron effective mass in semiconductor quantum wells under growth-direction applied magnetic fields"

Dios-Leyva, M., Porras-Montenegro, N., Brandi, H. S., and Oliveira, L. E.

The Ogg-McCombe effective Hamiltonian for the electron in the conduction band together with the nonparabolic and effective-mass approximations were used in a theoretical study of the cyclotron effective mass and electron effective Lande g(vertical bar vertical bar)-factor in semiconductor GaAs-Ga1-xAlxAs quantum wells under an applied magnetic field parallel to the growth direction of the quantum well. Calculations are performed as a function of the applied magnetic field, and for different widths of the GaAs-Ga1-xAlxAs quantum wells. Results for the electron cyclotron effective mass and g(vertical bar vertical bar)-factor are found in quite good agreement with experimental data

Brazilian Journal of Physics 36[3B], 854-857. 2006.

P 256- 06 "Electron spin resonance (ESR) and microwave absorption studies in TbMnO3 multiferroic compound"

Duque, J. G. S., Pagliuso, P. G., Rettori, C., Bufaical, L., Moreno, N. O., Urbano, R. R., and Kimura, T.

We report temperature dependent X-Band (f similar to 9.5 GHz) Electron Spin Resonance (ESR) and microwave absorption measurements in a single crystal of TbMnO3. A single Lorentzian ESR line with an isotropic g-value g similar to 1.96 was observed for T >= 120 K up to 600 K. The ESR signal is attributed to the Mn3+ ions in a insulator environment. The temperature dependence of the ESR linewidth is investigated for the external field applied along the three crystallographic axes. For all direction the ESR linewidth show a strong broadening as the temperature decreases due to the presence of short range magnetic correlations. The microwave absorption around the ferroelectric transition T-lock similar to 27 K was investigated using a special cavity with a TE103 mode where the sample sits at the maximum microwave electric-field

Ieee Transactions on Magnetics 42[10], 3084-3086. 2006.

P 257- 06 "Electronic excitation of H-2 by positron impact"

Arretche, F. and Lima, M. A. P.

Recent experiments on electronic excitation of molecules by positron impact have shown much larger cross sections than in the electron scattering case. The challenge of understanding the origin of this enhancement, especially just above electronic excitation thresholds, motivates the search of theoretical explanations of the phenomenon as well as new experimental efforts to confirm the data. In an earlier theoretical effort, an application of the Schwinger multichannel method at two-state level of approximation for the X (1)Sigma(+)(g)-> B (1)Sigma(+)(u) electronic excitation of the H-2 molecule, gave cross sections with smaller magnitude but reasonable qualitative agreement with the experimental data. The purpose of this work was to study the numerical stability of the previous calculation and to investigate the influence of open channels (energetically accessible electronic states-multichannel effects) and closed channels (energetically inaccessible electronic states-polarization effects) on this transition. Our results show minor multichannel effects and a significative enhancement of the X (1)Sigma(+)(g)-> B (1)Sigma(+)(u) cross section at the threshold due to polarization effects if compared to the usual static results

Physical Review A 74[4]. 2006.

P 258- 06 "Extra dimensions at the CERN LHC via mini-black holes: Effective KerrNewman brane-world effects"

Da Rocha, R. and Coimbra-Araujo, C. H.

We solve Einstein equations on the brane to derive the exact form of the brane-world-corrected perturbations in Kerr-Newman singularities, using Randall-Sundrum and Arkani-Hamed-Dimopoulos-Dvali (ADD) models. It is a consequence of such models that Kerr-Newman mini-black holes can be produced in LHC. We use this approach to derive a normalized correction for the Schwarzschild Myers-Perry radius of a static (4+n)-dimensional mini-black hole, using more realistic approaches arising from Kerr-Newman mini-black hole analysis. Besides, we prove that there are four Kerr-Newman black hole horizons in the brane-world scenario we use, although only the outer horizon is relevant in the physical measurable processes. Parton cross sections in LHC and Hawking temperature are also investigated as functions of Planck mass (in the LHC range 1-10 TeV), mini-black hole mass, and the number of large extra dimensions in brane-world large extra-dimensional scenarios. In this case a more realistic brane-effect-corrected formalism can achieve more precisely the effective extra-dimensional Planck mass and the number of large extra dimensions-in the Arkani-Hamed-Dimopoulos-Dvali model-or the size of the warped extra dimension-in Randall-Sundrum formalism

Physical Review D 74[5]. 2006.

P 259- 06 "Extracellular polymeric bacterial coverages as minimal area surfaces"

Saa, A. and Teschke, O.

Surfaces formed by extracellular polymeric substances enclosing individual and some small communities of Acidithiobacillus ferrooxidans on plates of hydrophobic silicon and hydrophilic mica are analyzed by means of atomic force microscopy imaging. Accurate nanoscale descriptions of such coverage surfaces are obtained. The good agreement with the predictions of a rather simple but realistic theoretical model allows us to conclude that they correspond, indeed, to minimal area (constant mean curvature) surfaces enclosing a given volume associated with the encased bacteria. This is, to the best of our knowledge, the first shape characterization of the coverage formed by these biomolecules, with potential applications to the study of biofilms.

Journal of Colloid and Interface Science 304[2], 554-557. 2006.

P 260-06 "Ferromagnetic state in ultrathin orthorhombic CrAs films: Thickness, lattice distortion, and half-metallic contributions"

Araujo, A. A., Laks, B., and de Camargo, P. C.

Orthorhombic CrAs thin films were investigated using first-principles spin-polarized calculations in the full-potential linearized augmented plane-wave method. Our results consider two different geometry optimization processes and show that the ferromagnetic state is favored by b-axis expansion, being more stable than the antiferromagnetic state for film thickness below approximately 24 A. The calculated maximum magnetic moment per formula unit is near 3 mu(B) and decreases with increasing film thickness, in good agreement with the observed saturation magnetization. The electronic structure of very thin films with expanded b axis suggests a half-metallic behavior

Physical Review B 74[17]. 2006.

P 261- 06 "Flavor coupled with chiral oscillations in the presence of an external magnetic field"

Bernardini, A. E.

Reporting to the Dirac wave-packet prescription where it is formally assumed the fermionic nature of the particles, we shall demonstrate that chiral oscillations implicitly aggregated to the interference between positive and negative frequency components of mass eigenstate wave-packets introduce some small modifications to the standard neutrino flavor conversion formula. Assuming the corresponding spinorial solutions of a 'modified' Dirac equation, we are specifically interested in quantifying flavor coupled with chiral oscillations for a fermionic Dirac-type particle (neutrino) non-minimally coupling with an external magnetic field B. The viability of the intermediate wave-packet treatment becomes clear when we assume B orthogonal/parallel to the direction of the propagating particle

European Physical Journal C 46[1], 113-122. 2006.

P 262- 06 "Fluctuation induced first-order phase transitions in a dipolar Ising ferromagnetic slab"

Fernandes, R. M. and Westfahl, H

We investigate the competition between the dipolar and the exchange interaction in a ferromagnetic slab with finite thickness and finite width. From an analytical approximate expression for the Ginzburg-Landau effective Hamiltonian, it is shown that, within a self-consistent Hartree approach, a stable modulated configuration arises. We study the transition between the disordered phase and two kinds of modulated configurations, namely, striped and bubble phases. Such transitions are of the first-order kind and the striped phase is shown to have lower energy and a higher spinodal limit than the bubble one. It is also observed that striped configurations corresponding to different modulation directions have different energies. The most stable are the ones in which the modulation vanishes along the unlimited direction, which is a prime effect of the slab's geometry together with the competition between the two distinct types of interaction. An application of this model to the domain structure of MnAs thin films grown over GaAs substrates is discussed and general qualitative properties are outlined and predicted, like the number of domains and the mean value of the modulation as functions of temperature

Physical Review B 74[14]. 2006.

P 263- 06 "Heat-induced charge transfer in cobalt iron cyanide"

Martinez-Garcia, R., Knobel, M., Goya, G., Gimenez, M. C., Romero, F. M., and Reguera, E.

The heating of Co(2+) ferricyanide above 80 degrees C induces an inner charge transfer from Co(2+) towards Fe(III) to form the mixed valence system Co(2+)Co(III) ferri- ferro-cyanide. This charge transfer takes place preserving the material framework and forming a solid solution of the initial and final species. The cell edge of the cubic cell (Fm-3m) of this solid solution follows a regular variation with the material composition. This mixed valence system was characterized using X-ray diffraction, infrared, thermo-gravimetric, Mossbauer and magnetic measurements. Its formation is easily detected by the appearance of an intermediate v(CN) absorption band in the infrared spectra at around 2120cm(-1), 40cm(-1) below and above the observed frequency for this vibration in Co(2+) ferri- and ferro-cyanide, respectively.
Journal of Physics and Chemistry of Solids 67[11], 2289-2299. 2006.

P 264- 06 "Kilohertz-resolution spectroscopy of cold atoms with an optical frequency comb"

Fortier, T. M., Le Coq, Y., Stalnaker, J. E., Ortega, D., Diddams, S. A., Oates, C. W., and Hollberg, L

We have performed sub-Doppler spectroscopy on the narrow intercombination line of cold calcium atoms using the amplified output of a femtosecond laser frequency comb. Injection locking of a 657-nm diode laser with a femtosecond comb allows for two regimes of amplification, one in which many lines of the comb are amplified, and one where a single line is predominantly amplified. The output of the laser in both regimes was used to perform kilohertz-level spectroscopy. This experiment demonstrates the potential for high-resolution absolute-frequency spectroscopy over the entire spectrum of the frequency comb output using a single high-finesse optical reference cavity

Physical Review Letters 97[16]. 2006.

P 265- 06 "Local and global magnetic properties of Zn1-xCoxO and Mn-doped GaAs thin films"

Iwamoto, W., Urbano, R. R., Pagliuso, P. G., Rettori, C., Samanta, K., Bhattacharya, P., Katiyar, R. S., da Silva, J. H. D., Pereira, A., Azevedo, G. D., and Oseroff, S. B.

Amorphous and crystalline thin films of Mn-doped(0.5%-10%) GaAs and crystalline thin films of Zn1-xCoxO(x = 3%-20%) were investigated by means of magnetic susceptibility and electron spin resonance (ESR). For the Mn-doped GaAs samples, our results show the absence of ferromagnetic ordering for the amorphous films in the 300 > T > 2 K temperature range, in contrast to the ferromagnetism found in crystalline films for T-C < 110 K. A single ESR line with a temperature independent g-value (g similar to 2) is observed for the amorphous films, and the behavior of this ESR linewidth depends on the level of crystallinity of the film. For the Mn-doped GaAs crystalline films, only a ferromagnetic mode is observed for T < TC when the film is ferromagnetic. Turning now the Zn1-xCoxO films, ferromagnetic loops were observed at room temperature for these films. The magnetization data show an increasing of the saturation magnetization M. as a function of x reaching a maximum value for x approximate to 10%. ESR experiments at T = 300 K in the same films show a strong anisotropic ferromagnetic mode (FMR) for x = 0.10

Ieee Transactions on Magnetics 42[10], 2700-2702. 2006.

P 266- 06 "Magnetic reconfiguration of MnAs/GaAs(001) observed by magnetic force microscopy and resonant soft x-ray scattering"

Coelho, L. N., Neves, B. R. A., Magalhaes-Paniago, R., Vicentin, F. C., Westfahl, H., Fernandes,R. M., Iikawa, F., Daweritz, L., Spezzani, C., and Sacchi, M.

We investigated the thermal evolution of the magnetic properties of MnAs epitaxial films grown on GaAs(001) during the coexistence of hexagonal/orthorhombic phases using polarized resonant (magnetic) soft x-ray scattering and magnetic force microscopy. The results of the diffuse satellite x-ray peaks were compared to those obtained by magnetic force microscopy and suggest a reorientation of ferromagnetic terraces as temperature rises. By measuring hysteresis loops at these peaks we show that this reorientation is common to all ferromagnetic terraces. The reorientation is explained by a simple model based on the shape anisotropy energy. Demagnetizing factors were calculated for different configurations suggested by the magnetic images. We noted that the magnetic moments flip from an in-plane monodomain orientation at lower temperatures to a three-domain out-of-plane configuration at higher temperatures. The transition was observed when the ferromagnetic stripe width L is equal to 2.9 times the film thickness d. This is in good agreement with the expected theoretical value of L=2.6d. (c) 2006 American Institute of Physics

Journal of Applied Physics 100[8]. 2006.

P 267- 06 "Magnetic study of nanoparticles of Mg0.95Mn0.05Fe2O4 spinel ferrite"

Sharma, S. K., Dolia, S. N., Kumar, R., Knobel, M., Kumar, V. V. S., and Singh, M.

Magnetization of nanoparticles of Mg-Mn ferrite, synthesized using high energy ball milling ha been studied. X-ray diffraction pattern of the particles milled for 6 h confirmed the single-phase cubic spinel structure with a lattice parameter of 8.47 angstrom. Langevin function fitting oil M-H data at 300K gives a log-normal particle size distribution with median diameter of 6.4 nm and standard deviation 0.7. The isothermal dc magnetization studies have been performed using SQUID and vibrating sample magnetorneter in the temperature range 5-300 K. These measurements show that the sample is superparamagnetic above the blocking temperature T-B similar to 246 K. The reduction in saturation magnetization in the case of nanoparticles has been explained on the basis that the magnetic moments in the surface layers outside the core are ill a state of frozen disorder

Indian Journal of Pure & Applied Physics 44[10], 771-773. 2006.

P 268- 06 "Magnetoresistivity as a probe to the field-induced change of magnetic entropy in RAl2 compounds (R=Pr,Nd,Tb,Dy,Ho,Er)"

Campoy, J. C. P., Plaza, E. J. R., Coelho, A. A., and Gama, S.

The heat capacity C-P(T) of the ferromagnetic compounds RAl2 (R=Pr,Nd,Tb,Dy,Ho,Er) was measured at zero and applied magnetic field of 5 T in the temperature interval from 2 to 200 K. From these results are calculated the magnetic component of the entropy change, -Delta S-mag(T)=S(0,T)-S(H,T). From resistivity measurements, rho(H,T), from 2 to 300 K in the same compounds, we calculated the resistivity change due to the applied magnetic field, -Delta rho(mag)(T)=[rho(mag)(0,T)-rho(mag)(H,T)]. The results are compared and we observed a similar dependence between -Delta rho(mag)(T) and (T/T-C)(m)Delta S-mag(T) with m=0 for T >= T-C and m=1 for T <= T-C. A simple model using a Hamiltonian considering molecular and crystalline electric fields, in a mean field approximation, is adopted for the calculus. Our results show that theory and experiment are in good agreement showing that the magnetoresistivity is a probe to the field-induced change of magnetic entropy in these compounds and can be extended to other materials. A model for the factor connecting both quantities, -Delta S-mag(T) and -Delta rho(mag)(T), is developed. This factor contains mainly the effective exchange integral which is related to Fermi energy that in turn is related to the electron effective mass

Physical Review B 74[13]. 2006.

P 269- 06 "Mechanical properties of amorphous nanosprings"

da Fonseca, A. F., Malta, C. P., and Galvao, D. S.

Helical amorphous nanosprings have attracted particular interest due to their special mechanical properties. In this work we present a simple model, within the framework of the Kirchhoff rod model, for investigating the structural properties of nanosprings having asymmetric cross section. We have derived expressions that can be used to obtain the Young's modulus and Poisson's ratio of the nanospring material composite. We also address the importance of the presence of a catalyst in the growth process of amorphous nanosprings in terms of the stability of helical rods

Nanotechnology 17[22], 5620-5626. 2006.

P 270- 06 "Metal-induced nanocrystalline structures in Ni containing amorphous silicon thin films"

Ferri, F. A., Zanatta, A. R., and Chambouleyron, I..

The mechanisms of silicon nanocrystal structure formation in amorphous Si films have been studied for a relative Ni impurity content varying between 0.1 and 10 at. %, i.e., from a Ni doping range to the Si-Ni alloy phase. The films, deposited by the cosputtering technique at 200 degrees C, were submitted to isochronal (15 min) annealing cycles up to 800 degrees C. Four different substrates were used to deposit the studied films: crystalline (c-) quartz, c-Si, c-Ge, and glass. Both the two orders of magnitude impurity concentration range variation and the very short annealing times were selected on purpose to investigate the first steps of the mechanism leading to the appearance of crystal seeds. The conclusions of this work are the following: (a) Ni impurity induces the low-temperature crystallization of amorphous silicon; (b) the NiSi2 silicide phase mediates, at the surface or in the bulk of the film, the crystallization process; and (c) the onset of crystallization and the crystalline fraction of the samples at each temperature depend not only on the Ni impurity concentration, but also on the nature of the substrate. (c) 2006 American Institute of Physics

Journal of Applied Physics 100[9]. 2006.

P 271- 06 "Model of workpiece erosion for electrical discharge machining process"

Sharakhovsky, L. I., Marotta, A., and Essiptchouk, A. M

The previously published step-wise model (SWM) of cold electrodes erosion of electric arc heaters (EAHs) was modified for the calculation of workpiece removal rate (WRR) in electrical discharge machining (EDM) process. Modified model applies both relations the step-wise erosion model and the point heat source erosion model and takes into account the discharge current, the discharge pulse/pause time and thermophysical properties of machined material. The results of calculations show a reasonable agreement with data obtained experimentally by different authors about different materials and conditions. (c) 2006 Elsevier B.V. All rights reserved

Applied Surface Science 253[2], 797-804. 2006.

P 272- 06 "Modeling the atomic structure of an amorphous Ni46Ti54 alloy produced by mechanical alloying using RMC simulations"

Gasperini, A. A. M., Machado, K. D., de Lima, J. C., and Grandi, T. A.

The local atomic order of an amorphous Ni46Ti54 alloy produced by Mechanical Alloying was studied by X-ray diffraction and modeled through reverse Monte Carlo simulations of its X-ray structure factor. From the simulations the partial pair distribution functions G(ij)(r) and partial structure factors S-ij(K) were determined and, from these functions, coordination numbers and interatomic distances for the first neighbors were calculated. The alloy shows a chemical short-range order and a preference for unlike pairs. The bond-angle distribution functions Theta(i-j-k)(cos theta) indicated that the local environment about Ni and Ti atoms are almost the same. (c) 2006 Elsevier B.V. All rights reserved

Chemical Physics Letters 430[1-3], 108-112. 2006.

P 273- 06 "Modification of the magnetic properties in molecular magnets based on Prussian blue analogues through adsorbed species"

Martinez-Garcia, R., Knobel, M., and Reguera, E.

The interaction of guest molecules (H2O, N-2, CO2, ethanol, methanol) with the metal ions at the pore surface in porous molecular magnets (M-3[Fe(CN)(6)](2)center dot xH(2)O, M = Mn, Co, Ni, Cu) was studied by x-ray diffraction, together with Mossbauer and magnetic data. These compounds can be dehydrated at relatively low temperature, usually below 100 degrees C. On the removal of water a cell contraction of about 4% of the cell volume is observed. This corresponds to a shortening of the metal-metal distance and to a strengthening for the metal-metal interaction through the CN bridge groups. In these materials the outer metal (M) is always found at the pore surface and the guest-host interactions modify the electronic structure of the host solid. Such interactions and their effect on the material electronic structure were studied by Mossbauer spectroscopy for the guest molecules mentioned. The most pronounced metal metal charge overlapping was observed for the host solid free of adsorbed species. When the guest molecules were absorbed the observed changes in the solid electronic structure followed the order N-2 similar to CO2 < ethanol < methanol < water. The most pronounced effect on the solid properties was observed for water, the most polar molecule within these guest species. The magnetic properties were evaluated for anhydrous and hydrated samples. The highest Curie temperature (T-C) and Curie-Weiss (theta(CW)) constant values were found for the anhydrous solids, when the metal at the pore surface only interacts with the CN bridge groups. This corresponds to an increase in the charge delocalization among metal centres on the removal of water, an effect already detected by x-ray diffraction and Mossbauer data. Since, during the water adsorption and desorption processes, the cell symmetry is preserved, such changes for the T-C and theta(CW) values cannot be ascribed to a variation in the linearity of the overlapping path. The observed effects are common to all the compounds studied and not to a particular metal ion. An explanation of such behaviour for the materials studied based on a tetrahedral coordination for the metal (M) linked at the N end of the CN groups in the anhydrous phase was discarded. In the cubic structure for Prussian blue analogues a true tetrahedral coordination cannot be present

Journal of Physics-Condensed Matter 18[49], 11243-11254. 2006.

P 274- 06 "Multipartite entanglement signature of quantum phase transitions"

de Oliveira, T. R., Rigolin, G., de Oliveira, M. C., and Miranda, E.

We derive a general relation between the nonanalyticities of the ground state energy and those of a subclass of the multipartite generalized global entanglement (GGE) measure defined by de Oliveira et al. [Phys. Rev. A 73, 010305(R) (2006)] for many-particle systems. We show that GGE signals both a critical point location and the order of a quantum phase transition (QPT). We also show that GGE allows us to study the relation between multipartite entanglement and QPTs, suggesting that multipartite but not bipartite entanglement is favored at the critical point. Finally, using GGE we were able, at a second-order QPT, to define a diverging entanglement length (EL) in terms of the usual correlation length. We exemplify this with the XY spin-1/2 chain and show that the EL is half the correlation length

Physical Review Letters 97[17]. 2006.

P 275- 06 "Nanocrystals of BaFe12O19 obtained by the proteic sol-gel process"

Fortes, S. S., Duque, J. G. S., and Macedo, M. A.

Nanocrystals of BaFe12O19, with a small amount of the BaFe2O4, were obtained by means of the proteic sol-gel process together. The results demonstrated that the magnetic and crystallographic properties are dependent on the calcination temperature and the values of M-r/M-s are very close to 0.5, which is the expected value by the Stoner-Wohlfarth model. The best calcination temperature was at 900 degrees C with M-s = 55.5 emu/g, H-c = 4.1 kOe and crystallite size 39 nm. (c) 2006 Elsevier B.V. All rights reserved

Physica B-Condensed Matter 384[1-2], 88-90. 2006.

P 276- 06 "Nitriding of AISI 4140 steel by a low energy broad ion source"

Ochoa, E. A., Figueroa, C. A., and Alvarez, F.

A comprehensive study of the thermochemical nitriding process of steel AISI 4140 by low energy ion implantation (Kaufmann cell). is reported. Different times of implantation were employed and the studied samples were characterized by x-ray diffraction, in situ photoemission electron spectroscopy, scanning electron microscopy, and hardness (nanoindentation) measurements. The linear relationship between nitrogen content and hardness was verified. The structure of the nitrided layer was characterized yielding that the compound layer is formed by coarse precipitates, around small grains, constituted principally by epsilon-Fe2-3N and gamma-Fe4N phases and the diffusion zone is formed by fine precipitates, around big grains of the original martensitic phase, constituted principally by gamma-Fe4N phase. Finally, a diffusion model for multiphase systems was applied to determine effective diffusion coefficients of nitrogen in the different phases.
Journal of Vacuum Science & Technology A 24[6], 2113-2116. 2006.

P 277- 06 "Nonlinear transport in n-III-nitrides: Selective amplification and emission of coherent LO phonons"

Rodrigues, C. G., Vasconcellos, A. R., and Luzzi, R.

The nonequilibrium, macrostate of the LO phonon system in strongly-polar n-doped III-nitrides, in the presence of electric fields of intermediate to high intensities, is characterized. The emergence of a kind of resonance consisting in the selective amplification of LO vibrations in a privileged and localized off-centre region of the Brillouin zone is demonstrated. It has an associated phenomenon akin to a Cherenkov-like effect involving a preferential emission of LO phonons in a selected cone with it's axis along the direction of the electric field. Moreover, it has predicted the onset of emission (stimulated amplification) of weakly decaying coherent LO phonons generated by the drifting electrons. (c) 2006 Elsevier Ltd. All rights reserved
Solid State Communications 140[3-4], 135-140. 2006.

P 278- 06 "Observation of muon neutrino disappearance with the MINOS detectors in the NuMI neutrino beam"

Michael, D. G. et. al

This Letter reports results from the MINOS experiment based on its initial exposure to neutrinos from the Fermilab NuMI beam. The rates and energy spectra of charged current nu(mu) interactions are compared in two detectors located along the beam axis at distances of 1 and 735 km. With 1.27x10(20) 120 GeV protons incident on the NuMI target, 215 events with energies below 30 GeV are observed at the Far Detector, compared to an expectation of 336 +/- 14 events. The data are consistent with nu(mu) disappearance via oscillations with vertical bar Delta m(32)(2)vertical bar=2.74(-0.26)(+0.44)x10(-3) eV(2) and sin(2)(2 theta(23))> 0.87 (68% C.L.)
Physical Review Letters 97[19]. 2006.

P 279- 06 "On Clifford subalgebras, spacetime splittings and applications"

Da Rocha, R. and Vaz, J.

Z(2)-gradings of Clifford algebras are reviewed and we shall be concerned with an alpha-grading based on the structure of inner automorphisms, which is closely related to the spacetime splitting, if we consider the standard conjugation map automorphism by an arbitrary, but fixed, splitting vector. After briefly sketching the orthogonal and parallel components of products of differential forms, where we introduce the parallel [orthogonal] part as the space [time] component, we provide a detailed exposition of the Dirac operator splitting and we show how the differential operator parallel and orthogonal components are related to the Lie derivative along the splitting vector and the angular momentum splitting bivector. We also introduce multivectorial-induced alpha-gradings and present the Dirac equation in terms of the spacetime splitting, where the Dirac spinor field is shown to be a direct sum of two quaternions. We point out some possible physical applications of the formalism developed

International Journal of Geometric Methods in Modern Physics 3[7], 1359-1380. 2006.

P 280- 06 "Optical conductivity of charge carriers interacting with a two-level systems reservoir"

Ferrer, A. V., Caldeira, A. O., and Smith, C. M.

Using the functional-integral method we investigate the effective dynamics of a charged particle coupled to a set of two-level systems as a function of temperature and external electric field. The optical conductivity and the direct current (dc) resistivity induced by the reservoir are computed. Three different regimes are found depending on the two-level system spectral function, which may lead to a non-Drude optical conductivity in a certain range of parameters. Our results contrast to the behavior found when considering the usual bath of harmonic oscillators which we are able to recover in the limit of very low temperatures

Physical Review B 74[18]. 2006.

P 281- 06 "Phenomenological analysis connecting proton-proton and antiproton proton elastic scattering"

Avila, R. F., Campos, S. D., Menon, M. J., and Montanha, J.

Based on the behavior of the elastic scattering data, we introduce an almost model-independent parameterization for the imaginary part of the scattering amplitude, with the energy and momentum transfer dependences inferred on an empirical basis and. selected by rigorous theorems and bounds from axiomatic quantum field theory. The corresponding real part is analytically evaluated by means of dispersion relations, allowing connections between particle-particle and particle-antiparticle scattering. Simultaneous fits to proton-proton and antiproton-proton experimental data in the forward direction and also including data beyond the forward direction lead to a predictive formalism in both energy and momentum transfer. We compare our extrapolations with predictions from some popular models and discuss the applicability of the results in the normalization of elastic rates that can be extracted from present and future accelerator experiments (Tevatron, RHIC and LHC)

European Physical Journal C 47[1], 171-186. 2006.

P 282- 06 "Piezoelectric coefficients d(14), d(16), d(34) and d(36) of an L-arginine hydrochloride monohydrate crystal by X-ray three-beam diffraction"

Almeida, J. M. A., Miranda, M. A. R., Avanci, L. H., de Menezes, A.S., Cardoso, L. P., and Sasaki, J. M.

Previous work employed X-ray three-beam diffraction techniques to obtain part of the L-arginine hydrochloride monohydrate (L-AHCL. H2O) piezoelectric coefficients, namely d(21), d(22), d(23) and d(25). Those coefficients were obtained by measuring the shift in the angular position of a number of secondary reflections as a function of the electric field applied in the [010] piezoelectric direction. In this paper a similar procedure has been used to measure the remaining four piezoelectric coefficients in L-AHCL. H2O: with the electric field applied in the [100] direction, d(14) and d(16) were measured; with the electric field applied in the [001] direction, d(34) and d(36) were obtained. Therefore the entire piezoelectric matrix of the L-AHCL. H2O crystal has been successfully measured

Journal of Synchrotron Radiation 13, 435-439. 2006.

P 283- 06 "Previous heat treatment inducing different plasma nitriding behaviors in martensitic stainless steels"

Figueroa, C. A., Alvarez, F., Mitchell, D. R. G., Collins, G. A., and Short, K. T.

In this work we report a study of the induced changes in structure and corrosion behavior of martensitic stainless steels nitrided by plasma immersion ion implantation (PI3) at different previous heat treatments. The samples were characterized by x-ray diffraction and glancing angle x-ray diffraction, scanning electron microscopy, energy dispersive x-ray spectroscopy, and potentiodynamic measurements. Depending on the proportion of retained austenite in the unimplanted material, different phase transformations are obtained at lower and intermediate temperatures of nitrogen implantation. At higher temperatures, the great mobility of the chromium yields CrN segregations like spots in random distribution, and the alpha'-martensite is degraded to alpha-Fe (ferrite). The nitrided layer thickness follows a fairly linear relationship with the temperature and a parabolic law with the process time. The corrosion resistance depends strongly on chromium segregation from the martensitic matrix, as a result of the formation of CrN during the nitrogen implantation process and the formation of CrxC during the heat treatment process. Briefly speaking, the best results are obtained using low tempering temperature and low implantation temperature (below 375 degrees) due to the increment of the corrosion resistance and nitrogen dissolution in the structure with not too high diffusion depths (about 5-10 mu m). (c) 2006 American Vacuum Society

Journal of Vacuum Science & Technology A 24[5], 1795-1801.2006.

P 284- 06 "Radial distribution of internal stresses in as-quenched FeCoSiB amorphous wire analyzed through giant magnetoimpedance"

Canola, D. B., Duque, J. G. S., and Knobel, M.

The dependence of the giant magnetoimpedance effect on both the applied tensile stress and skin depth is employed to estimate the average,of the frozen-in stresses within a Co-based amorphous wire fabricated by the in-rotating water quenching technique. In order to estimate the average stress in different regions of the wire (cylindrical shells), selected frequencies of the driving current were applied, which give rise to different effective skin depths. Experimental results display a continuous increase of the frozen-in stresses from the centre to the surface of the wire, confirming that the fabrication process indeed introduces a radial magnetoelastic anisotropy distribution. (c) 2006 Elsevier B.V. All rights reserved

Physica B-Condensed Matter 384[1-2], 158-161. 2006.

P 285- 06 "Relativistic models of galaxies"

Vogt, D. and Letelier, P. S.

A special form of the isotropic metric in cylindrical coordinates is used to construct what may be interpreted as the general relativistic versions of some well-known potential-density pairs used in Newtonian gravity to model three-dimensional distributions of matter in galaxies. The components of the energy-momentum tensor are calculated for the first two Miyamoto-Nagai potentials and a particular potential due to Satoh. The three potentials yield distributions of matter in which all tensions are pressures and all energy conditions are satisfied for certain ranges of the free parameters. A few non-planar geodesic orbits are computed for one of the potentials and compared with the Newtonian case. Rotation is also incorporated in the models and the effects of the source rotation on the rotation profile are calculated as first-order corrections by using an approximate form of the Kerr metric in isotropic coordinates

Monthly Notices of the Royal Astronomical Society 363[1], 268-284. 2005.

P 286- 06 "SrFe12O19 prepared by the proteic sol-gel process"

Brito, P. C. A., Gomes, R. F., Duque, J. G. S., and Macedo, M. A.

Powders of strontium hexaferrite (SrFe12O19) were prepared by the proteic sol-gel process using coconut water as a precursor. X-ray diffraction (XRD) measurement showed the formation of SrFe12O19 with a small amount of the hematite for the sample calcined at 1000 degrees C with Fe/Sr = 12. Rietveld refinement disclosed that this sample had 87.56% of the SrFe12O19 and 12.44% of Fe2O3 and the values for R-p, R-wp and chi(2) were 4.28%, 5.93% and 1.71, respectively. The magnetic properties were M-s = 64 emu/g, M-r/M-s, = 0.55 and H-c = 1.4 kOe for a crystallite size of 57 nm. (c) 2006 Elsevier B.V. All rights reserved

Physica B-Condensed Matter 384[1-2], 91-93. 2006.

P 287- 06 "Statistical approach to non-Fickian diffusion"

Vasconcellos, A. R., Ramos, J. G., Gorenstein, A., Kleinke, M. U., Cruz, T. G. S., and Luzzi, R.

Competing styles in statistical mechanics have been introduced to investigate physicochemical systems displaying complex structures, when one faces difficulties to handle the standard formalism in the well-established Boltzmann-Gibbs statistics. After a brief description of the question, we consider the particular case of Renyi statistical approach, which is applied to the study of the "anomalous" (non-Fickian) diffusion that is involved in experiments of cyclic voltammetry in electro-physical chemistry. In these experiments, one is dealing with the fractal-like structure of the thin film morphology present in electrodes in microbatteries. Fractional-power laws axe evidenced in the voltammetry measurements and in the analysis of the interphase width obtained using atomic force microscopy. The resulting fractional-powers are related to each other and to the statistical fractal dimension, and can be expressed in terms of the index on which Renyi's statistical approach depends. The important fact that this index, which is restricted to a given interval, provides a measure of the micro-roughness of the electrode surface, and is related to the dynamics involved, the nonequilibrium thermodynamic state of the system, and to the experimental protocol is clarified

International Journal of Modern Physics B 20[28], 4821-4841. 2006.

P 288- 06 "Structurally tuned magnetic properties of TbmRhnIn3m+2n (m-1, 2; n=0, 1) intermetallic antiferromagnets"

Lora-Serrano, R., Ferreira, L. M., Garcia, D. J., Miranda, E., Giles, C., Duque, J. G. S., Granado, E., and Pagliuso, P. G.

We report the evolution of the magnetic properties of a new series of intermetallic compounds TbmRhnIn3m+2n (m = 1, 2; n = 0, 1) which are structurally related to a class of Ce-based heavy-fermion superconductors (HFS). Measurements of temperature-dependent magnetic susceptibility, specific heat and X-ray resonant magnetic scattering (XRMS) were performed on single crystalline samples of TbIn3, TbRhIn5 and Tb2RhIn8. The tetragonal materials TbRhIn5 and Tb2RhIn8 both order antiferromagnetically with higher ordering temperatures (T-N = 45.5 and 42.8 K, respectively) than their cubic relative TbIn3 (T-N = 32.7 K). Their commensurate magnetic structure and the direction of Tb magnetic moments will be discussed in terms of crystalline electrical field (CEF) effects and Ruderman-Kittel-Kasuya-Yoshida (RKKY) interaction with effects of magnetic frustration being released by lower dimensionality. A more general picture about the role of CEF in determining the magnetic properties of other R-based members of these series is discussed. (c) 2006 Elsevier B.V. All rights reserved

Physica B-Condensed Matter 384[1-2], 326-328. 2006.

P 289- 06 "Structure and energetics of molecular point defects in ice I-h"

de Koning, M., Antonelli, A., da Silva, A. J. R., and Fazzio, A.

We present a first-principles study of the molecular vacancy and three distinct molecular interstitial structures in ice I-h. The results indicate that, due to its bonding to the surrounding hydrogen-bond network, the bond-center (Bc) configuration is the favored molecular interstitial in ice I-h. A comparison between the vacancy and the Bc interstitial suggests that the former is the predominant molecular point defect for T less than or similar to 200K although a crossover scenario in which the latter becomes favored below the melting point is conceivable

Physical Review Letters 97[15]. 2006.

P 290- 06 "Study of the Kondo and high-temperature limits of the slave-boson and X boson methods"

Nunes, L. H. C. M., Figueira, M. S., and Foglio, M. E.

In this Letter we study the periodic Anderson model, employing both the slave-boson and the X-boson approaches in the mean field approximation. We investigate the breakdown of the slave-boson at intermediate temperatures when the total occupation number of particles N-t = N-f + N-c is keep constant, where N-f and N-c are respectively the occupation numbers of the localized and conduction electrons, and we show that the high-temperature limit of the slave-boson is N-f = N-c = N-t/2. We also compare the results of the two approaches in the Kondo limit and we show that at low-temperatures the X-boson exhibits a phase transition, from the Kondo heavy fermion (K-HF) regime to a local moment magnetic regime (LMM).

Physics Letters A 358[4], 313-321. 2006.

P 291- 06 "Study on optimum fiber length for maximum gain in C- and L-band EDFAs"

Rieznik, A. A., Fragnito, H. L., Silva, M. B. C. E., and der Weid, J. P.

We study the optimum fiber length for maximum gain of C- and L-band Erbium Doped Fiber Amplifiers (EDFAs) with fixed pump power. We show that the dependence of the optimum length on the wavelength and power of the signal is stronger in the L than in the C band and validate our findings trough distributed gain measurements. We also show that the predictions of the transcendental power equation model, which neglects the Amplified Spontaneous Emission (ASE), give accurate results for the optimum length even of L-band EDFAs, fact not obvious a priori because of the key rule played by the ASE as a pump source in amplifiers operating in this region. (c) 2006 Elsevier B.V. All rights reserved

Optics Communications 266[2], 546-551. 2006.

P 292- 06 "Superconductivity in a new quaternary phase with HgSM0.5In0.5Pb2 composition"

Corsini, R., Bortolozo, A. D., da Luz, M. S., da Silva, R. R., dos Santos, C. A. M., and Machado, A. J. S.

This work reports a systematic study on the structural and superconducting properties in the Hg-Sm-In-Pb system. It is investigated how In and Sm dopings influence the superconducting properties of the HgPb2 phase which was recently reported. Results for the HgSm1-xPb2 system show that Sm atoms substitute Hg vacancies in the tetragonal phase which do not affect the onset critical temperature of the HgPb2 compound. Simultaneous Sm and In doping effects on the properties of the HgPb2 phase are also studied. Experimental and simulations of X-ray powder diffractograms suggest that the HgSm1-xInxPb2 system (0.2 <= x <= 0.7) has a pseudo-cubic structure with lattice parameters near 4.88 angstrom. Superconducting properties measurements show that this system has an optimum doping at x similar to 0.5 with the onset critical temperature close to 6.9 K. This is the highest superconducting critical temperature for the AuCu prototype so far reported.

Materials Letters 61[1], 263-266. 2007.

P 293- 06 "Suppression and coherent control of free-induction-decay emission in multilevel systems"

de Araujo, L. E. E.

In this paper, I study the coherent control and suppression of the free-induction-decay emission associated with the decay from an excited multilevel atom to its ground state. It is shown here that a strong and ultrashort coupling pulse, resonant with the excited states and a lower state other than the ground state, can induce destructive quantum interferences in the decay process. The suppression is temporary and the free-induction-decay signal reappears one quantum-beat period (of the excited states) later. A sequence of equally spaced, ultrashort coupling pulses can control the moment the free-induction-decay emission occurs

Physical Review A 74[4]. 2006.

P 294- 06 "Surface properties and cell behaviour of diamond-like carbon coatings produced by plasma immersion"

Uzumaki, E. T., Lambert, C. S., Santos, A. R., and Zavaglia, C. A. C

The morphology, microstructure and roughness of the diamond-like carbon (DLC) films produced by plasma immersion were investigated. Vero cells (fibroblasts) were utilized for the in vitro biocompatibility studies of the DLC-coated Ti-13Nb-13Zr alloy. In the cytotoxicity assay, fibroblast cells were cultured for a period of 24 h, and in the adhesion assay, cells were cultured for a period of 2 and 24 h. The cell morphology was investigated by scanning electron microscopy (SEM) and atomic force microscopy (AFM). No evidence was found that the presence of the DLC coating had any adverse effect. Our results show that the adherence of fibroblasts was significantly enhanced when Ti alloy was coated with DLC from the uncoated.

Thin Solid Films 515[1], 293-300. 2006.

P 295- 06 "Survival probability of large rapidity gaps in a QCD model with a dynamical infrared mass scale"

Luna, E. G. S.

We compute the survival probability {vertical bar S vertical bar(2)} of large rapidity gaps (LRG) in a QCD based eikonal model with a dynamical gluon mass, where this dynamical infrared mass scale represents the onset of nonperturbative contributions to the diffractive hadron-hadron scattering. Since rapidity gaps can occur in the case of Higgs boson production via fusion of electroweak bosons, we focus on WW -> H fusion processes and show that the resulting {vertical bar S vertical bar(2)} decreases with the increase of the energy of the incoming hadrons; in line with the available experimental data for LRG. We obtain {vertical bar S vertical bar(2)} = 27.6 +/- 7.8% (18.2 +/- 17.0%) at Tevatron (CERN-LHC) energy for a dynamical gluon mass m(g) = 400 MeV.

Physics Letters B 641[2], 171-176. 2006.

P 296- 06 "Synthesis and X-ray structural characterization of NiO nanoparticles obtained through gelatin"

Maia, A. O. G., Meneses, C. T., Menezes, A. S., Flores, W. H., Melo, D. M. A., and Sasaki, J. M.

Nanoparticles of fcc-NiO phase were obtained by heating the dried resin resultant of a mixture of gelatin and NiCl2 center dot 6H(2)O in aqueous solution. The average particle size and microstrain were calculated from the line broadening of X-ray powder diffraction peaks, and these values were between 15 nm and 78 nm, and 0.056% and 0.172%, respectively. The Rietveld refinement method was applied to all diffraction patterns. The particle size, obtained from this procedure, changes as a function of temperature, heating time and the remarkable reduction due to the addition of NaOH to the solution, which can be attributed to the presence of NaCl crystals and carbon encapsulating NiO nanoparticles during the heating. The heating temperature was in the range of 350-700 degrees C. Thermo-gravimetric analysis showed that the majority of organic fraction starts to disappear after 300 degrees C.

Journal of Non-Crystalline Solids 352[32-35], 3729-3733. 2006.

P 297- 06 "The calculation of free-energies in semiconductors: Defects, transitionsand phase diagrams"

Hernandez, E. R., Antonelli, A., Colombo, L., and Ordejon, P.

In this chapter we review a series of novel techniques that make possible the efficient calculation of free energies in condensed-matter systems, without resorting to the quasiharmonic approximation. Employing these techniques, it is possible to obtain the free energy of a given system not just at a predefined temperature, but in a whole range of temperatures, from a single simulation. This makes possible the study of phase transitions, as well as the determination of equilibrium concentrations of defects as a function of temperature, as will be illustrated by examples of specific applications. The same techniques, coupled with a scheme to integrate the Clausius-Clapeyron equation, can lead to the efficient determination of phase diagrams, a capability that will be illustrated with the calculation of the phase diagram of silicon

Theory of Defects in Semiconductors 104, 115-139. 2007.

P 298- 06 "The effect of Ge implantation dose on the optical properties of Ge nanocrystals in SiO2"

Mestanza, S. N. M., Rodriguez, E., and Frateschi, N. C.

Ge nanocrystallites (Ge-nc) embedded in a SiO2 matrix are investigated using Raman spectroscopy, photoluminescence and Fourier transform infrared spectroscopy. The samples were prepared by ion implantation with different implantation doses (0.5, 0.8, 1, 2, 3 and 4) X 10(16) cm(-2) using 250 keV energy. After implantation, the samples were annealed at 1000 degrees C in a forming gas atmosphere for I h. All samples show a broad Raman spectrum centred at omega approximate to 304 cm(-1) with a slight shift depending on the implantation doses. The Raman intensity also depends on the Ge74+ dose. A maximum photoluminescence intensity is observed for the sample implanted at room temperature with a dose of 2 x 10(16) cm(-2) at 3.2 eV. Infrared spectroscopy shows that the SiO2 films moved off stoichiometry due to Ge74+ ion implantation, and Ge oxides are formed in it. This result is shown as a reduction of GeOx, at exactly the dose corresponding to the maximum blue-violet PL emission and the largest Raman emission at 304 cm(-1). Finally, the Raman spectra were fitted with a theoretical expression to evaluate the average size, full-width at half-maximum (FWHM) and dispersion of Ge-nc size

Nanotechnology 17[18], 4548-4553. 2006.

P 299- 06 "The exotic characteristics of Centauro-I: a model to describe Centauro-I"

Ohsawa, A., Shibuya, E. H., and Tamada, M.

In our previous paper on Centauro-I (Ohsawa et al 2004 Phys. Rev. D 70 074028), we showed that the shower cluster, found in the block 112 of the lower chamber, is produced in the target layer by a number of hadrons with appreciable lateral spread. These hadrons are accompanied by no (or one at most) gamma-ray(s) with energy above detection threshold, and produce no shower in the upper chamber but 28 visible C-jets (with the visible energy more than 2 TeV) in the target layer. These characteristics are quite exotic and unable to be described by a fluctuation of ordinary atmospheric families. In the present paper, we propose a model of strange quark matter (SQM) among the primary cosmic rays to describe the exotic features of the event. A large SQM droplet enters the atmosphere and fragments into a bundle of small strangelets in the atmosphere without emission of gamma-rays, and these small strangelets explode into nucleons in the upper chamber. The number of collisions in the upper chamber is estimated to be as small as 3-4 in contrast to 20-30 collisions in the target layer. We discuss the intensity of Centauro-I together with the exotic events observed by the balloon and satellite experiments, which were also ascribed to strange quark matter

Journal of Physics G-Nuclear and Particle Physics 32[11], 2333-2344. 2006.

P 300- 06 "The gauge boson masses for a minimal SU(4)(EW)circle times U(1)(B-l) model for electroweak interactions with left-right symmetry"

Bernardini, A. E.

Following the general procedure of spontaneous symmetry breaking of a SU(4)(EW) circle times U(1)(B-l) electroweak gauge group with left-right symmetry, we obtain the gauge boson masses and currents for the minimal version of the model. The physical eigenstates for neutral gauge bosons are determined by introducing two mixing angles theta(4) and theta(3) which are related to the electroweak mixing angle theta(w) at the unification scale. By introducing some physical approaches in order to simplify the calculations, we calculate the charged and neutral currents. Differently from other previous propositions, the results are obtained from a theoretical constraint upon the coupling constants as a consequence of embedding the symmetry into the Pati-Salam electroweak coupling SU(4)(EW) circle times SU(4)(PS)

Journal of Physics G-Nuclear and Particle Physics 32[11], 2313-2332. 2006.

P 301- 06 "Theoretical study of electron collisions with the CF2 radical"

Lee, M. T., Iga, I., Machado, L. E., Brescansin, L. M., Castro, E. A. Y., and de Souza, G. L. C.

In this work, a theoretical study on electron-CF2 collisions in the low and intermediate energy range is reported. More specifically, calculated elastic differential, integral and momentum transfer cross sections, as well as total absorption cross sections are presented in the (1-500) eV energy range. A complex optical potential is used to represent the electron-molecule interaction dynamics, whereas the iterative Schwinger variational method combined with the distorted-wave approximation is used to solve the scattering equations. A comparison of the present results is made with the available theoretical and experimental results for electron collisions with CF2 as well as with O-3 (an isoelectronic molecule of CF2)

Physical Review A 74[5]. 2006.

P 302- 06 "Thermodynamics of type-I and type-II Si clathrates at zero pressure: Monte Carlo simulations"

Miranda, C. R. and Antonelli, A.

We have investigated the thermodynamic and structural properties of types I and II silicon clathrates through Monte Carlo simulations. Using efficient methods to determine free energies, we studied the stable and metastable relations between the various phases of Si, namely, crystalline, liquid, amorphous, and the two types of clathrates, at zero pressure. We determined the melting point of Si-46 (type I) and Si-34 (type II) clathrate structures to be at 1482 +/- 25 and 1522 +/- 25 K, respectively. Our result for the melting point of Si-34 is in good agreement with the experimental value of 1473 K. Our results also indicate that both clathrate forms are more stable than amorphous silicon for any temperature up to their melting point

Physical Review B 74[15]. 2006.

P 303- 06 "Thermotropic phase behavior of DPPC liposome systems in the presence of the anti-cancer agent 'Ellipticine'"

Cavalcanti, L. P. and Torriani, I. L.

This letter presents our first results on the structural changes in DPPC multilamellar vesicles dispersed in water in the presence of the anti-cancer agent Ellipticine. The thermotropic phase transitions of the lamellar packing inside lipid vesicles were characterized in situ by small angle X ray diffraction. The results lead to the determination of a critical concentration value for drug loading on the vesicle system around 4% molar fraction of Ellipticine, an indication of the localization of the drug in the alkyl chains and the influence of the drug on the decreasing rate of the bilayer period after the main phase transition

European Biophysics Journal with Biophysics Letters 36[1], 67-71. 2006.

P 304- 06 "Transmission electron microscopy and molecular dynamics study of the formation of suspended copper linear atomic chains"

Sato, F., Moreira, A. S., Bettini, J., Coura, P. Z., Dantas, S. O., Ugarte, D., and Galvao, D. S.

We report high-resolution transmission electron microscopy and molecular dynamics simulation results of mechanically stretching nanowires leading to linear atomic suspended chain (LAC) formation. In contrast with some previous experimental and theoretical works in the literature that stated that the formation of LAC's for copper should be unlikely our results showed the existence of LAC's for the [111], [110], and [100] crystallographic directions, being thus the sequence of most probable occurrence. Our results clearly indicate that temperture and pulling velocity, associated with internal stress, are fundamental aspects to determine LAC formation

Physical Review B 74[19]. 2006.

P 305- 06 "Transverse magnetic anisotropy of magnetoelastic origin induced in Co nanowires"

Silva, E. L., Nunes, W. C., Knobel, M., Denardin, J. C., Zanchet, D., Pirota, K., Navas, D., and Vazquez, M.

The magnetic properties of arrays of magnetic nanowires, prepared by electrodeposition in nanopores of alumina membranes, were investigated. The hysteresis loops were measured using a magnetic field applied both perpendicularly and parallel to the nanowire axes for temperatures between 4 and 300 K. The results show a preferred direction of magnetization parallel to the nanowire axis at room temperature, but perpendicular to the nanowire axis below a certain crossover temperature. We observe that such crossover temperature increases by increasing the nanowire length. The results are discussed considering strains caused by the different expansion coefficients of the nanowires and the matrix. (c) 2006 Elsevier B.V. All rights reserved

Physica B-Condensed Matter 384[1-2], 22-24. 2006.

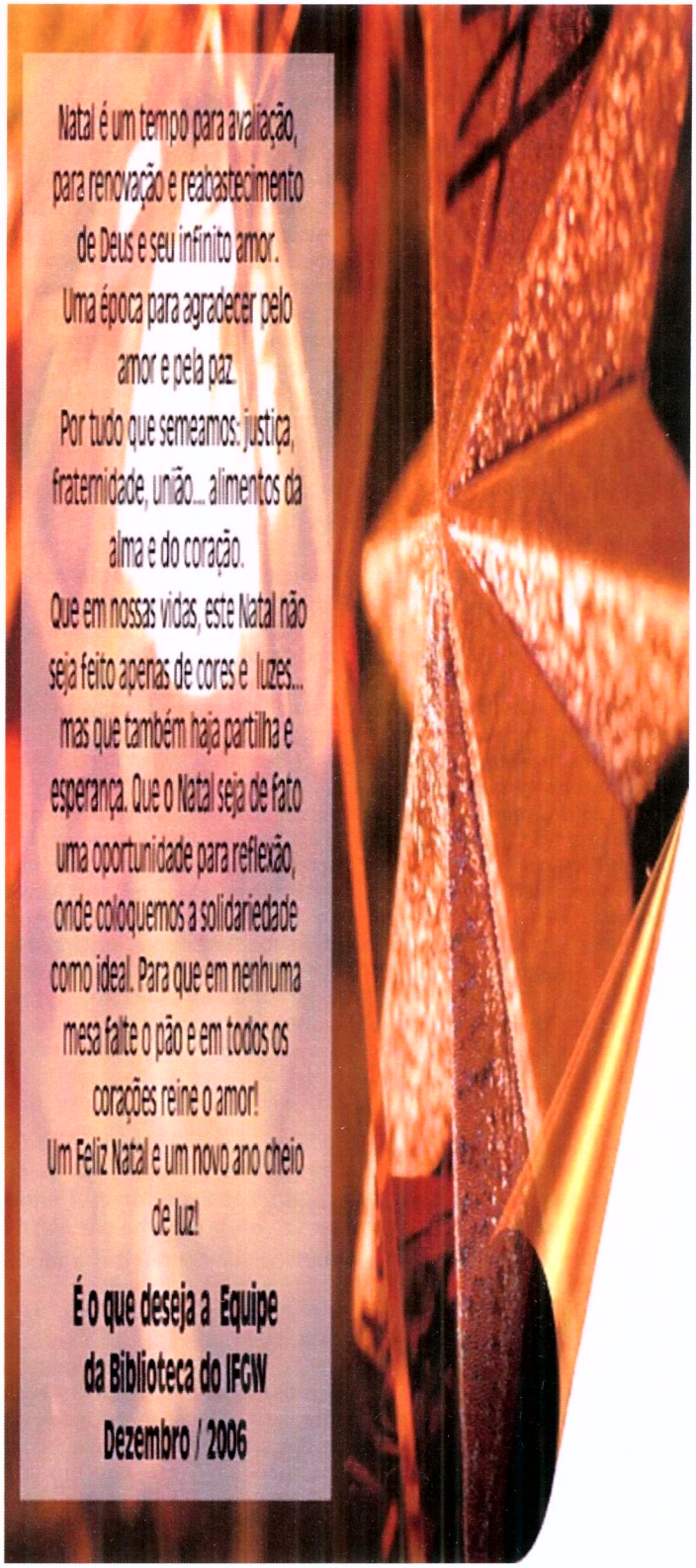

Abstracta

Instituto de Física
Diretor: Prof. Dr. Júlio César Hadler Neto
Universidade Estadual de Campinas - UNICAMP
Cidade Universitária C.P. 6165
CEP: 13081-970 - Campinas - SP - Brasil
e-mail: secdir@ifi.unicamp.br
Fone: 0XX 193521-5300 / Fax: 0XX 19 3521-3127

Publicação

Biblioteca do Instituto de Física Gleb Wataghin
http://www.ifi.unicamp.br/bif
Diretora Técnica: Rita Aparecida Sponchiado

Elaboração
Tânia Macedo Folegatti
abstract@ifi.unicamp.br

Projeto Gráfico
ÍgneaDesign

Impressão
Gráfica Central - Unicamp